International Journal of Manufacturing Economics and Management
ISSN 2784-1278 ISSN-L 2784-1278, Vol. V, No. 2 / 2025
https://doi.org/10.54684/ijmem.2025.5.2.6

ANALYSIS OF THERMAL CONDITIONS DURING WAAM ADDITIVE MANUFACTURING

Aleksander Lisiecki[1,2], Barbara Balon[1], Fedeles Mihai-Alexandru[3], Dediu Costel[3], Simona-Nicoleta Mazurchevici[3], Ciprian Ciofu[4], Dumitru Nedelcu[3], Shuyang Qin[5], Yujiao Ke[6], Yevgenia Chvertko[7], Marek Wycisło[1], Maksymilian Ziebura[1]

[1]Silesian University of Technology, Faculty of Mechanical Engineering, Konarskiego 18A, 44-100 Gliwice, Poland
[2]Łukasiewicz Research Network – Upper Silesian Institute of Technology, Centre of Welding, K. Miarki 12, 44-100, Gliwice, Poland
[3]"Gheorghe Asachi" Technical University of Iasi, Department of Machine Manufacturing Technology, Blvd. Mangeron, No. 59A, 700050, Iasi, Romania
[4]"Gheorghe Asachi" Technical University of Iasi, Faculty of Mechanical Engineering, Blvd. Mangeron 61-63, 700050, Iasi
[5]National Engineering Research Center for Equipment and Technology of Cold Strip Rolling, Yanshan University, Qinhuangdao 066004, P.R. China
[6]School of Mechanical Engineering, Yanshan University, Qinhuangdao, 066004, P.R. China
[7]Welding Department, National Technical University of Ukraine "Igor Sikorsky Kyiv Polytechnic Institute", 37, Prospect Beresteiskyi, 03056 Kyiv, Ukraine

Corresponding author: Aleksander Lisiecki, aleksander.lisiecki@polsl.pl

Abstract: The article presents an original methodology for testing thermal conditions in the WAAM additive manufacturing process using a thermal imaging camera. The study was conducted by producing vertical test walls during robotic arc deposition of 1.0 mm diameter unalloyed steel wire on a steel starting plate. After deposition, a thermal image of the wall was taken, and point measurements were conducted using a thermocouple. Measurements were also taken of the height of each bead and the wall height increase. As a result of the study and analysis of thermal conditions, the thermal cooling cycles of individual beads were determined under various deposition parameters (energy input). The structure and microstructure of the cross-sections of the walls were also determined. The developed thermal conditions research methodology can be used to predict wall deposition conditions or to adaptively control the robotic WAAM manufacturing process.
Keywords: WAAM manufacturing process, thermal conditions, thermal image.

1. INTRODUCTION

Additive manufacturing (AM), also referred to as 3D printing, is regarded as a significant advancement in manufacturing technology of the 20th century and is highly esteemed by numerous nations. It incorporates numerous advanced technologies, including digital modeling, material processing, machining, and metallurgical engineering. Additive manufacturing (AM) provides substantial benefits in conserving raw materials and minimizing processing cycles by depositing material layer by layer under computer control. From an economic and management standpoint, these benefits lead to diminished tooling expenses, abbreviated lead times, and more flexibility in production planning, especially for bespoke or low-volume manufacturing. Specifically, it can manufacture intricately shaped components with exceptional precision, eliminating the dependence on cutting tools, fixtures, dies, and many intricate procedures necessitated by conventional machining. Consequently, it has garnered significant attention in aircraft, biology, energy, the chemical industry, and micro-nano manufacturing, among others [1, 2].
Currently, additive manufacturing is the focal point of industry and research owing to several advancements in techniques and technologies. This is further reinforced by the prevailing trend towards resource efficiency, as additive manufacturing processes have the potential for near net shape or net shape production. For cost-intensive materials such as titanium or tungsten, additive manufacturing may be the preferred production method. This material efficiency directly influences production costs and sustainability metrics, which are increasingly pertinent in strategic manufacturing management. The primary criteria affecting the choice of additive manufacturing technique include the achievable complexity and resolution, deposition rate, and

component size, as seen in Figure 1. Additive manufacturing provides significantly greater design flexibility compared to traditional manufacturing methods, enabling load-optimized design possibilities. Wire arc additive manufacturing (WAAM) is a potential field of additive manufacturing that use an electric arc in conjunction with wire as the deposition medium for production. This procedure is a component of direct energy deposition (DED) production, which encompasses techniques such as laser cladding. In 2020, direct energy deposition technologies accounted for 16% of the additive manufacturing market. The expanding market share of DED underscores its rising industrial significance and investment appeal. Compared to other metal additive manufacturing processes, WAAM has reduced cooling rates and increased heat input. This is advantageous for the majority of commercially accessible materials. Moreover, the deposition rates and part dimensions can be enhanced due to the diminished complexity and surface quality of the component relative to powder bed-based additive manufacturing procedures, as illustrated in Figure 1. WAAM refers to all wire-based additive manufacturing techniques that utilize arc welding. The extensive study in arc welding for surfacing and joint welding has resulted in a comprehensive understanding of material and process behavior, allowing for the application of established basics. The distinction between conventional joint welding using arc welding techniques and additive manufacturing was effectively demonstrated by Mohebbi et al., Cunningham et al., and others, and may be encapsulated as a variance in the heat conduction of the material, [4, 5].

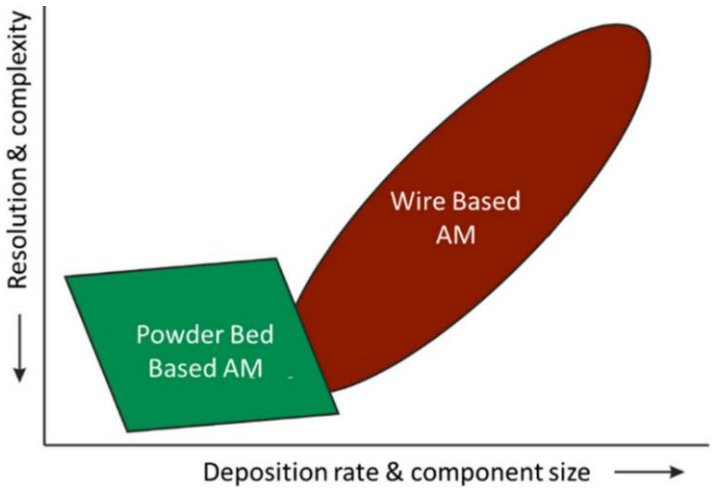

Fig. 1. Correlation across wire-based and powder bed-based AM, [3]

In joint welding, thermal conductivity occurs in multiple dimensions (Figure 2(a)), whereas in WAAM processes, heat is primarily conducted in a single direction: toward the bottom of the part (Figure 2(b)) [3-5].

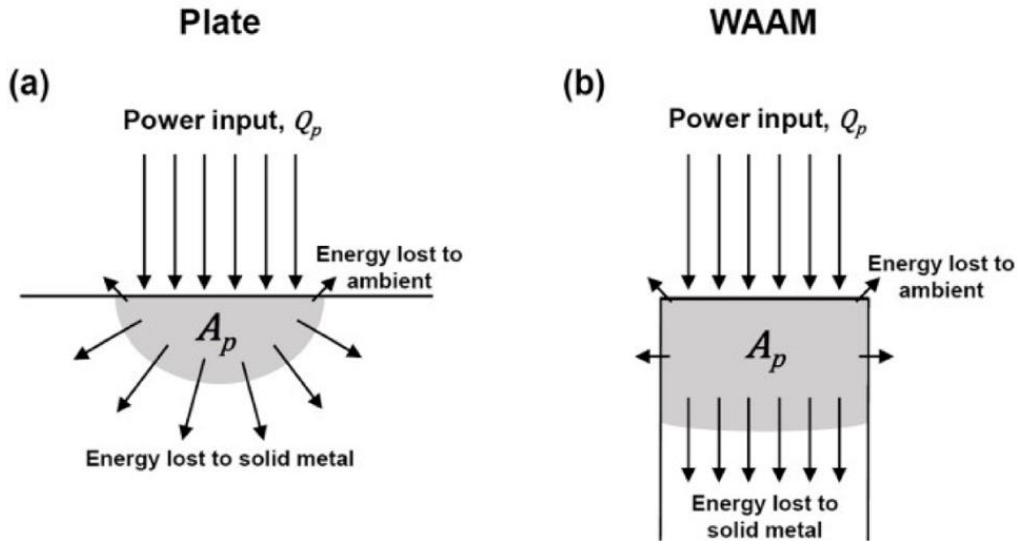

Fig. 2. Heat transfer in joint welding and wire arc additive manufacturing (WAAM). (a) Thermal conductivity occurs in multiple dimensions; (b) thermal conductivity occurs in a single direction, [4]

Figure 3 shows the first WAAM-made bridge realized in four parts and combined with non-welded parts. It has a weight of 7.8 t and a welded weight of 4.6 t, [6].

Fig. 3. WAAM - created bridge, [6]

The bridge effectively demonstrates the feasibility of producing organic-looking components, which are typically challenging to create using traditional manufacturing methods. New design rules are being developed and implemented in university teaching globally. Greer et al. demonstrated the application of novel design principles for a section of a crane arm, resulting in a component that is lighter than its conventionally produced counterpart, [7]. Kulikov et al. demonstrated the feasibility of manufacturing compressor impellers using WAAM and outlined the entire process chain, highlighting the advantages of WAAM over traditional impeller manufacturing methods, as noted in reference [8]. Bergmann et al. demonstrated this in the context of manufacturing a steel knot for construction applications [9]. Panchenko et al. evaluated the advantages of WAAM relative to other additive manufacturing processes, as illustrated in a structured diagram in Figure 4, [10]. Roy et al. identified several key advantages of wire arc additive manufacturing, including reduced lead time, minimized material waste, enhanced functionality, tailored tooling for low-volume components, and the potential for multi-material design [11].

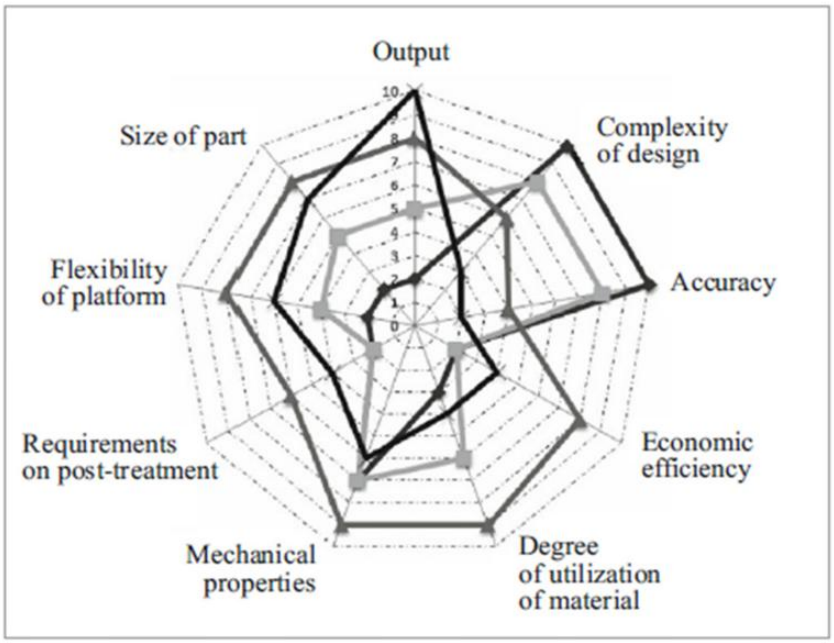

◆) bed deposition; ■) direct deposition; ×) electron beam freeform fabrication; ▲) WAAM.

Fig. 4. Benefits of WAAM and various additive manufacturing techniques, [10]

2. ADDITIVE MANUFACTURING PROCESSES FOR METALS

Metal additive manufacturing processes can be generally categorized into powder-based and wire-based methods, depending on the form of the material feed utilized. A further essential classification examines the

approach to energy delivery, differentiating between processes that utilize localized heating and those that employ localized material deposition. Powder bed fusion processes involve a volume that is gradually filled with metal powder, which is then locally scanned by a heat source like a laser or electron beam, exemplifying a localized heating method. Conversely, direct energy deposition processes entail the localized deposition of material, wherein material is propelled towards a melting pool created by the interaction of a heating source with the substrate. Composite extrusion modeling represents a specific approach within material extrusion, employing thermoplastic wires that are significantly filled with metal powder. Figure 5 illustrates the different classifications of metal additive manufacturing processes, as referenced in sources [1, 2].

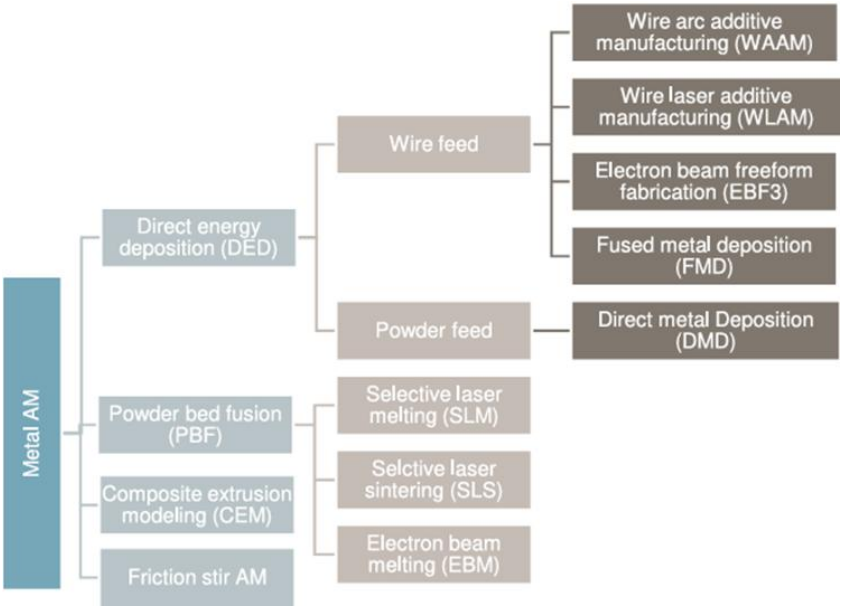

Fig. 5. Classification of metal additive manufacturing processes, [2]

From a management and economic viewpoint, this “process taxonomy” serves as a procurement and investment framework: each category entails specific capital expenditures (equipment), operational expenses (consumables/energy), qualification costs, and risk profiles (powder handling, safety, and compliance), which directly affect the total cost of ownership and make-or-buy choices.

2.1. Powder bed fusion

Powder bed fusion (PBF) processes utilize an energy source, usually a laser or electron beam, to sinter or melt metal particles that are spread throughout a building chamber, as illustrated in Figure 6. The procedure necessitates specific apparatus such as a vacuum chamber for electron beam melting, a heated chamber to minimize thermal distortions, metal powder particles, and a powder roller. The procedure consists of three main stages: the initial phase involves the platform moving backward across a layer height of 50–100 μm; the second phase includes the distribution of fresh powder from the stock chamber over the build chamber using a powder roller; and the final phase entails scanning the layer with the energy source. The build process often experiences considerable downtime because of the necessity for powder spreading, as achieving uniform powder distribution is essential for maintaining print quality. This requires comparatively moderate roller blade speeds. In addition to this limitation, PBF processes encounter various challenges, such as the requirement for specialized powders that possess particular characteristics related to particle size distribution, flowability, and chemical composition. Ensuring uniformity in powder quality poses a considerable operational hurdle and financial concern. The necessity for accurate build chamber leveling to ensure consistent layer deposition and dimensional precision presents continuous operational difficulties. The utilization of high-energy sources (200–1000 W for lasers, up to 10 kW for electron beams) adds layers of complexity to equipment management and safety protocols, [1].
From an economic perspective, these constraints result in increased indirect costs, including downtime, powder quality assurance and quality control, rework or scrap, and environmental health and safety compliance. Consequently, business cases for powder bed fusion frequently depend on high value density components, consistent demand, and robust utilization rates.

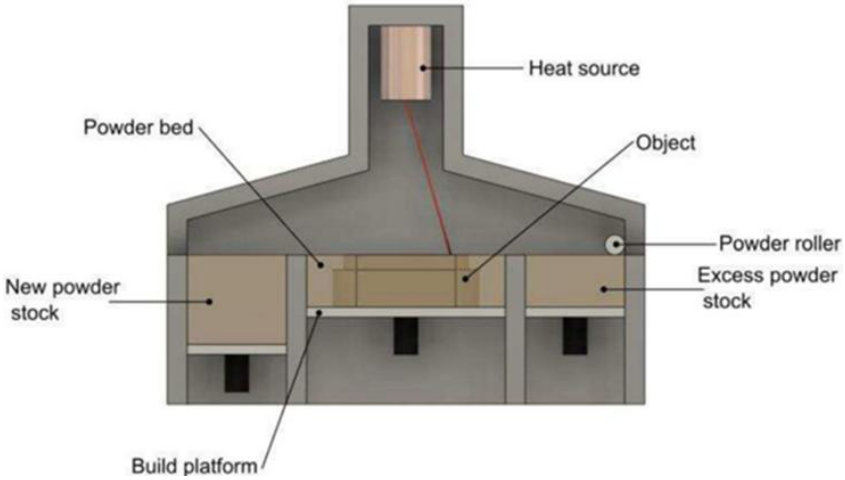

Fig. 6. Illustration of the PBF technique, [1]

2.2. Direct energy deposition

Direct energy deposition (DED) techniques utilize an energy source, such as a laser, electron beam, or electric arc, in conjunction with feedstock material presented as powder or wire. The procedure utilizes a torch head, shielding gas, and, where applicable, a carrier gas for powder feedstock. During operation, the heat source liquefies a thin layer of the substrate in conjunction with the locally deposited material. The melt pool is safeguarded from ambient gases by shielding gas delivered directly from the laser or torch head. In contrast to PBF, DED functions in an unobstructed environment and can be easily executed with robotic motion systems. Utilizing powder feedstock in Directed Energy Deposition (DED) presents various constraints, including the reliance on costly heat sources, diminished precision relative to alternative additive manufacturing methods, increased distortion from quick cooling, and inferior surface uniformity. The issues are exacerbated by the intricacies of powder management and upkeep. Wire arc additive manufacturing (WAAM), utilizing wire feedstock material, offers a feasible option. WAAM has considerable benefits compared to powder-based DED, such as reduced equipment and feedstock expenses, streamlined material management, elevated deposition rates, and enhanced productivity. Nonetheless, WAAM has specific drawbacks, such as diminished precision relative to DED, heightened distortion resulting from the lack of heated chambers, inferior surface uniformity, and challenges with arc stability. The increased wire diameter utilized in WAAM constrains the attainable resolution and feature size capabilities. Figure 7 depicts the concept of the Direct Energy Deposition (DED) method utilizing wire feed material [1, 2, 3, 5].

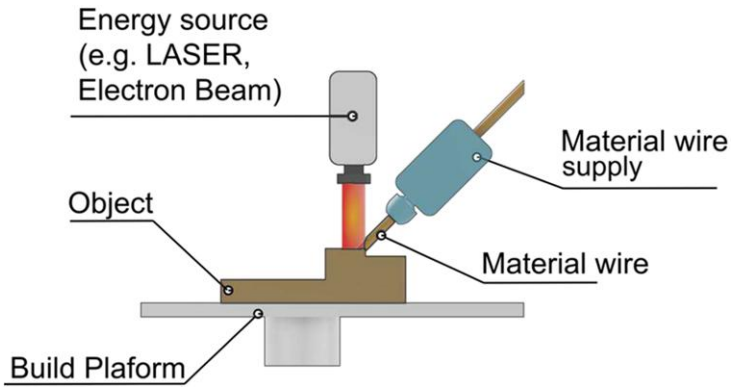

Fig. 7. Illustration of the DED technique, wire feed material [1]

From a managerial perspective, the comparison between WAAM and powder-DED often involves a trade-off between throughput and surface finish/precision. Companies frequently implement a "near-net + machining" operational model, reallocating costs from production time to subsequent finishing and quality assurance, which should be incorporated into standard costing and capacity planning.

2.3. Composite extrusion modeling

Composite extrusion modeling (CEM) uses thermoplastic filaments densely infused with metal powder, generally comprising over 95% powder by weight. The procedure utilizes a cost-effective material extrusion

apparatus to create a "green part," which then undergoes debinding and sintering to yield the final metal component. CEM offers the benefit of utilizing inexpensive equipment; however, it encounters other constraints, such as limited material availability, difficulties in preserving structural integrity—especially for intricate geometries—and issues with dimensional accuracy. The procedure entails three separate stages: printing, debinding, and sintering, hence increasing the complexity of the production process, as seen in Figure 8. Moreover, non-uniform shrinkage during debinding and sintering must be carefully addressed to achieve a satisfactory component shape. The limited attainable part dimensions, due to distortions during debinding and sintering, constitute another major constraint of the process, [1, 2].

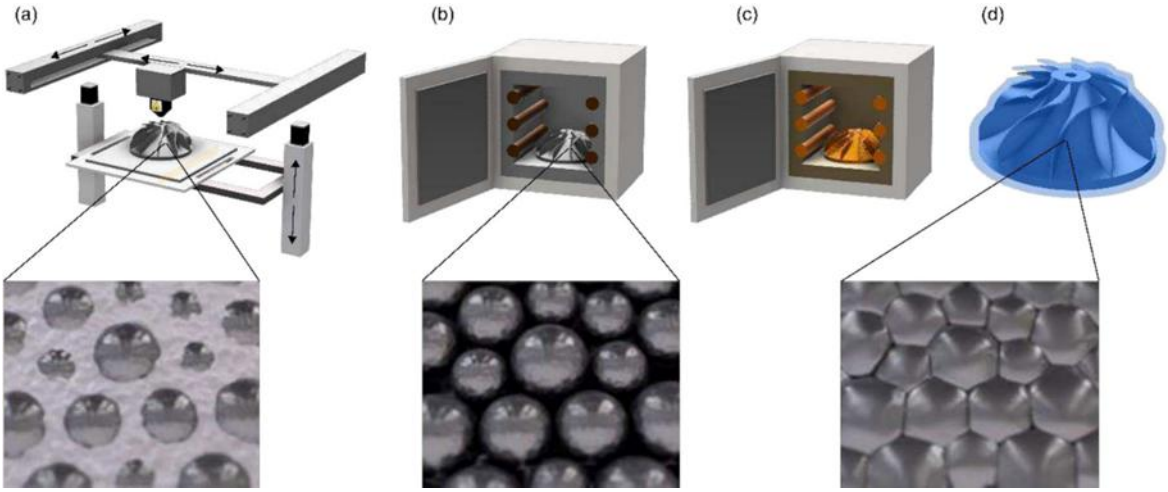

Fig. 8. Composite extrusion modeling process: (a) 3D printing of the green component, (b) debinding of the green component in a debinding furnace, (c) sintering of the resultant brown component, [12]

From an operations management perspective, the three-step process elevates work-in-progress and lead time variability; hence, adherence to scheduling and the optimization of yield learning curves are essential for attaining competitive unit prices.

2.4. Friction stir additive manufacturing

Friction stir additive manufacturing (FSAM) functions analogously to friction stir welding, employing a consumable rod that rotates and advances toward the substrate to deposit material in a semi-solid condition. This method presents numerous benefits compared to traditional DED procedures, owing to its reduced operating temperature and energy usage. The augmented pressure and agitation facilitate the attainment of high-strength components characterized by a refined microstructure and less porosity or gas inclusions. Lower operating temperatures relative to fusion-based processes lead to less distortion and minimal residual strains. Furthermore, FSAM has extensive material compatibility, especially with aluminum, steel, and other alloys. Nonetheless, FSAM has considerable constraints. The approach has rather sluggish build speeds relative to conventional additive manufacturing methods, which may restrict its use in quick production contexts. The intricacy of the equipment and the related expenses may hinder wider adoption, especially among smaller businesses. Achieving surface finish quality can be difficult, frequently necessitating post-processing procedures. Moreover, FSAM is constrained in its ability to fabricate intricate geometries, demonstrating greater appropriateness for components with uncomplicated forms, as illustrated in Figure 9, [13].

FSAM can be strategically positioned as a "quality-first" option (minimizing defects and residual stress) for businesses where lifecycle cost and reliability are paramount in purchasing decisions; this influences pricing strategy, warranty risk, and certification timelines.

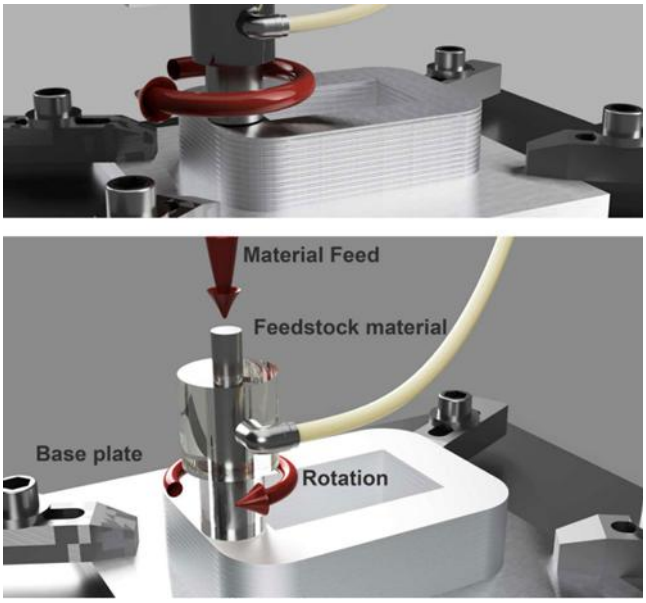

Fig. 9. Illustration of the FSAM technique, [12]

3. WIRE ARC ADDITIVE MANUFACTURING

3.1. Advantages of WAAM

WAAM possesses the capability to offer a cost-efficient method for producing massive metal structures, hence obviating the need for costly and time-consuming castings and forgings. Diverse technologies are vying for market dominance in large-scale metal additive manufacturing, each possessing distinct advantages and limitations. WAAM has been chosen as the preferred deposition technique due to its inherent advantages:

• A high deposition rate is attainable for WAAM.

• Quality feedstock is accessible, yielding excellent mechanical qualities and achieving 100% density.

WAAM does not inherently necessitate a fully sealed container, therefore theoretically allowing for an unbounded part size.

• WAAM can yield substantial cost reductions owing to the comparatively low expense and intricacy of the robots, machinery, and power sources, [2, 3, 5].

Additional benefits can be observed in enhancing the component's structure to mitigate stress concentration, hence decreasing its overall weight and environmental footprint. Future lightweight, intricate, and topology-optimized component designs can be produced with WAAM, [3, 7, 9]. Cranfield University has engaged in WAAM process development for over fifteen years, alongside part fabrication utilizing various techniques and materials. Component production necessitates comprehensive expertise to attain precise geometry devoid of distortion and flaws. Most prior research emphasizes the fabrication of uncomplicated structures, such as walls and non-intersecting components, sometimes overlooking the complexities involved in producing large-scale elements, [2, 3, 5].

The most compelling applications of WAAM in management and economics are frequently associated with (i) enhanced supply chain resilience through diminished reliance on forging and casting lead times, (ii) reduction of working capital via near-net material savings, and (iii) expedited engineering change cycles, which can enhance time-to-market and decrease design iteration costs.

3.2. Numerical simulations for WAAM processes

Current studies indicate that WAAM simulations generally span meso-scale and macro-scale dimensions. Simulations at the meso-scale concentrate on the temporary behavior of weld pool creation and the processes of solidification. They utilize thermo-fluidic techniques to analyze the intricate thermal and fluid dynamics at play. Conversely, macro-scale simulations focus on the comprehensive structural temperature fluctuations and deformations. They mainly employ thermo-mechanical techniques for computation, [14, 15].

Thermo-fluidic modeling. The thermo-fluidic models in WAAM aim to replicate the complex thermal and fluid dynamics that occur throughout the manufacturing process. These models facilitate the acquisition of transient multi-physics field data, which can frequently present challenges or be unattainable through experimental approaches. Insights are also provided regarding the behaviors of molten pools when subjected to different material compositions and welding parameters. The external structural morphology and functional attributes of

the workpiece are influenced by these factors, [15].
Essential stages in thermo-fluidic modelling. Thermo-fluidic modeling employs CFD simulations to tackle the complex physical phenomena observed in WAAM. The study of arc welding has significantly enhanced the comprehension of these intricate thermal and fluid flow issues. This modeling technique excels in forecasting phenomena related to the flow and solidification of molten materials during WAAM, encompassing heat transfer, mass transfer, and fluctuations at the free surface. Figure 10 illustrates the standard CFD simulation workflow for WAAM, which consists of six steps: geometry modelling, physics modelling, setting boundary conditions, spatial discretization, solution, and results analysis, [15].

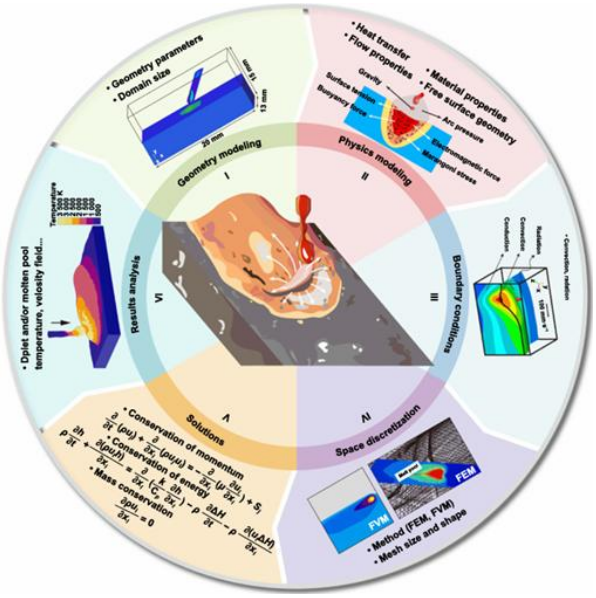

Fig. 10. Standard procedure for thermo-fluidic simulation, [14]

3.3. Future perspective

This section delineates several promising avenues for further exploration and improvements in simulation techniques for WAAM, grounded in the analysis of methodologies, applications, and identified challenges. The components encompass high-quality data acquisition, the application of ML to simulations, the integration of simulation into WAAM DTs, cloud computing, and advanced software development, [14, 15].
From a management perspective, these directions align with the value drivers of the latest industrial revolution: the availability of data facilitates key performance indicators and governance; machine learning and digital technologies support closed-loop control; cloud computing provides scalable processing power; and software ecosystems influence vendor lock-in, cybersecurity, and the development of organizational capabilities.
High-quality data acquisition: Obtaining high-quality data poses considerable difficulties, especially in light of the demanding operational conditions established by WAAM processes. The conditions in these environments significantly restrict the ability to collect precise data. The elevated temperatures produced during WAAM pose challenges for the application of thermocouples that are welded onto deposition layers in proximity to the dynamic heat source. Contact-based thermocouples are commonly employed to assess the temperature at the baseplate of the workpiece for the purpose of model validation. As the layer height increases, accurately validating temperatures further from the baseplate presents challenges. The use of non-contact pyrometers or thermal cameras allows for temperature measurements at various surface locations; however, the significant smoke generated during welding activities poses challenges in accurately capturing real temperature data. Furthermore, the data processing stage presents significant challenges in efficiently filtering out contaminants. For example, when collecting data on welding pool or arc shapes, the clarity of image-based information can be affected by the intensity of the arc, unless proper filtering is applied. This frequently necessitates the extraction of geometric features from raw images, a challenge that can be particularly daunting for WAAM designers lacking significant expertise in data management and feature extraction. Methods like modifying emissivity and reducing noise can enhance data quality; however, they remain reliant on thorough preliminary experiments and calculations. The necessity for accurate simulations renders high-quality data essential. Future advancements should prioritize the creation of equipment and algorithms capable of enduring complex operational conditions while also efficiently reducing contamination, thereby guaranteeing the collection of dependable data, [15].
From an economic perspective, improved data minimizes the “cost of poor quality” associated with scrap, rework, and warranty risks, while also facilitating scalable certification and traceability, which are crucial for

the aerospace and energy supply chains.

Applying ML to simulations: The combination of machine learning and simulations establishes a mutually beneficial framework, with each component amplifying the strengths of the other. Machine learning assists in uncovering unknown parameters essential for the development of simulations, whereas the results from simulations contribute to the training of machine learning models. These models consist of algorithms that derive decision-making rules from data. They are capable of forecasting physical states across diverse parameter configurations and intricate geometries, tackling issues associated with computational demands and the range of simulation relevance. Firstly, machine learning excels at addressing inverse problems, which entails extracting unknown physical principles from data. This capability is especially significant for deducing crucial yet hard-to-pinpoint simulation parameters, including high-temperature material properties and characteristics of heat sources. For instance, Liao et al. employed a physics-informed machine learning model to ascertain unknown material properties such as heat capacity and conductivity, [16]. In a similar vein, Pereira and Alvarez et al presented an offline/online data assimilation approach aimed at forecasting uncertain parameters, such as the geometry of double ellipsoid heat sources and energy absorptivity, [17]. Furthermore, simulation outcomes can serve as a foundational theory for the training of machine learning models, equipping them with robust generalization abilities. The ability to perform these tasks is crucial for developing parametric maps and forecasting intricate geometric structures, areas where existing simulations face challenges. One method entails creating intricate models via traditional simulation by breaking them down into more manageable components. Following this, machine learning can be utilized to understand and incorporate the material behavior and deformation results of these models within the wire arc additive manufacturing process. The progress in machine learning has confirmed its capabilities and importance in fluid dynamics and various additive manufacturing fields. Recent studies in the WAAM field, although limited, have shown that the integration of ML with simulation provides enhanced flexibility and efficiency in predictive performance. This approach not only aids in building models based on parameters before executing the simulation but also leverages the predictive insights that arise from the simulations. This raises a crucial inquiry: is it possible for machine learning to enhance the simulation process itself? Enhancing the evolution of next-generation ML algorithms that excel in intelligence, speed, and physical transparency continues to be a primary area of investigation, [15-17].

In the realm of management, the integration of machine learning and simulation alters the required skill set, combining data engineering with manufacturing engineering. This evolution shifts the competitive edge toward organizations capable of effectively implementing models through operational practices, validation, and governance, rather than merely focusing on prototype development.

Integrating simulation into DTs: DTs present a compelling approach to improve the precision of WAAM simulations. Characterized by their integrated multi-physics and multi-scale virtual representations, these systems utilize the most effective physical models to replicate real-world processes. Within the framework of WAAM, digital twins mainly enable the real-time simulation, monitoring, and regulation of manufacturing equipment and products. Computational multi-physics modelling acts as a fundamental element of the DT framework and provides significant educational benefits. Simulations offer crucial physical theories that support the understanding and development of decision trees. Nonetheless, conventional simulations frequently struggle to effectively manage the stochastic variables inherent in the physical environment. There are challenges in aligning updates with the real-time WAAM process, potentially resulting in a gradual deviation from the actual outcomes. Moreover, simulations are unable to deliver real-time predictive outcomes for digital twins because of their significant computational requirements. DTs facilitate the ongoing prediction of state variables and the forecasting of future conditions by utilizing real-time sensing data. For example, Mu et al. created a DT framework that relies on numerical simulation to build an online deformation prediction model, [18]. Dynamic systems, such as DTs, are not fixed models; they undergo continuous updates and adjustments by incorporating real-time data from the additive manufacturing process, including temperature, velocity, and distortion. In the event of discrepancies during the manufacturing process, the DT can promptly modify its forecasting and simulation parameters to align with the revised manufacturing scenario. This mechanism for real-time prediction updates guarantees that the model remains in sync with the actual manufacturing process. Furthermore, by consistently acquiring knowledge from its physical equivalent, a digital twin gradually enhances its depiction of the physical entity as time progresses. The ongoing advancement of digital twins in the additive manufacturing sector is primarily theoretical at this stage; however, their capacity for virtual testing, optimization, real-time process monitoring, and dynamic adjustments holds considerable promise. The study and application of DTs are expected to emerge as a significant focus within the WAAM field. In the interim, if advancements are made in efforts to enhance simulations, it could become possible to perform real-time simulations, thereby providing digital twins with essential predictive information, [15, 18].

The adoption of digital transformation is economically justified when it minimizes variability and stabilizes throughput, leading to less unplanned downtime and fewer rejected builds. This results in predictable delivery performance, which has become an increasingly vital key performance indicator in contract manufacturing and aerospace/defense supply chains.

Cloud computing: Cloud computing offers an effective approach to address the computational challenges in WAAM, providing low capital costs and access to high-performance computing resources. This approach serves as a method of distributed computing, offering scalable and on-demand access to vast computing resources, encompassing processing power and data storage, via the Internet. This technology enables the segmentation of extensive data processing tasks into smaller, more manageable components. The components are subsequently allocated throughout a cloud network and handled by a multi-server architecture. In the context of WAAM, the computational requirements can be quite high, indicating that local or edge computing devices may fall short in terms of effective data processing and storage capabilities. The utilization of cloud computing has the potential to greatly accelerate simulation processes, meet substantial data storage requirements, and improve the handling of large datasets produced during WAAM simulations. Numerous investigations have utilized cloud-level simulations to identify defects and forecast material behaviors in WAAM. For instance, intricate tasks like multi-scale, high-resolution modeling of crack propagation and failure mechanisms significantly leverage the advantages of cloud computing capabilities. Additionally, Miras et al employed cloud computing for Monte Carlo simulations, significantly decreasing the simulation duration from 30 hours to merely 48 minutes, [18]. Therefore, leveraging cloud infrastructure alongside edge computing devices constitutes a strategic method to enhance the computational power of edge devices by utilizing the strong resources provided by cloud computing. This collaboration not only speeds up computational processes but also improves the overall efficiency and scalability of simulations in WAAM, [18].

From a management perspective, transitioning to the cloud reallocates expenditures from capital to operational expenses; therefore, it is essential for procurement and finance to assess pay-per-use costs, data sovereignty, and cybersecurity measures within the operating framework.

Advanced software development: Creating specialized simulation software for WAAM is essential for progressing industrial applications and scholarly pursuits. Industrial users gain advantages from simulation software tailored to their specific requirements, providing straightforward mastery and intuitive interfaces. Conversely, the academic community necessitates advanced simulation software that offers open access to comprehensive intermediate variables and a versatile programming environment. At present, the available simulation software does not sufficiently address the requirements of either sector. The software for industrial users often exhibits excessive complexity, featuring a multitude of modules that cover diverse areas, including spring Maxwell modules and composite damage modules, which may not have direct applicability to WAAM applications. Many industrial users require simulations that are uncomplicated and easy to use. Moreover, the specific language employed in these modules can pose difficulties in comprehension. This requires a design that incorporates a clear and concise user interface, along with modules specifically tailored for WAAM requirements. The challenge faced involves limited data accessibility and the lack of transparency regarding how software models and predict various process outcomes. This frequently arises from limitations set by proprietary software platforms. As many individuals in this field do not engage in the creation of foundational algorithms in software engineering, they might encounter challenges when it comes to debugging and analyzing results. Moreover, the lack of dedicated simulation software for WAAM compels users across various expertise levels to undertake intricate programming to create WAAM simulations. In LS-DYNA, WAAM materials are not easily selectable, necessitating that users define material properties on an individual basis. In ANSYS, users face challenges due to the absence of an advanced simulation plugin for WAAM, necessitating independent management of tasks like defining the heat source and planning the path for executing WAAM simulations. Tackling these challenges necessitates sophisticated simulation software that improves data accessibility, integrates detailed WAAM process models, and provides a completely programmable environment for skilled users. Reaching these objectives will necessitate collaboration across various disciplines, engaging specialists from fields such as computer science, materials science, physics, and interface design, among others. This collaborative effort is crucial to guarantee that the software is both technically sound and user-friendly, addressing real-world manufacturing challenges effectively, [15]. From an organizational perspective, “software for WAAM” transforms into a capability asset: the processes of vendor selection, training, IP management (including custom plugins/scripts), and change management are critical in deciding if simulation serves merely as a one-time engineering tool or evolves into a consistent production system.

4. MATERIALS AND METHODS

The main goal of the study was to analyse the thermal conditions of the WAAM additive manufacturing process by arc deposition of steel wire using spot temperature measurements and thermal imaging. The analysis included determining the temperature distribution along and across the single bead/layer, determining maximum temperature values, and characterizing the cooling rates of single and multi-bead layers.
For the WAAM additive manufacturing test, starting plates were made of S235 structural steel samples wit dimensions 220x150x10 mm. The starting plate was used to initiate the 3D printing process and position the printed components. The starting plate material should be similar to the deposited material.
The material used for 3D printing tests using the WAAM method was ESAB OK Autrod 12.51 (0.10% C, 1.11% Mn, 0.72% Si) solid wire with a diameter of 1.0 mm. It is a copper-plated welding wire with the addition of manganese and silicon, intended for MIG/MAG welding of unalloyed and low-carbon structural steel.
According to the manufacturer, the chemical composition of the wire has been optimized to ensure a stable welding arc, reduce spatter levels, and ensure good wetting of the substrate by the weld pool, which is particularly important in additive manufacturing processes such as WAAM, where it is crucial to ensure repeatability of the shape, dimensions, and quality of individual layers.
According to the manufacturer, the mechanical properties of the deposit include a yield strength of 430-480 MPa, tensile strength of 530-590 MPa, and relative elongation of up to 30%, depending on the shielding gas used. According to recommendations, welding can be carried out in pure CO_2 as well as in mixtures of argon and carbon dioxide, e.g., 80% Ar + 20% CO_2. For additive manufacturing tests, the M21 mixture (82% Ar + 18% CO_2) was used.
Tests of additive manufacturing by arc deposition of steel wire were performed on a robotic welding cell. The cell consisted of a FANUC Arc Mate 100iC welding robot (4), a FANUC R-30iA control system (1), a Castolin Eutectic TotalArc2 5000 welding power source (6), a Fronius VR 1500 4R/W/D Roboter wire feeder (5), an OK Autrod 12.51 wire spool, a DINSE T. Connector HW DIX RETZ 663 SAZ welding torch, and shielding gas delivery system fo the mixture of 82% Ar + 18% CO_2, a Kemper Smart Master welding gas extraction system (2), and table for mounting the samples (3), Fig. 11.

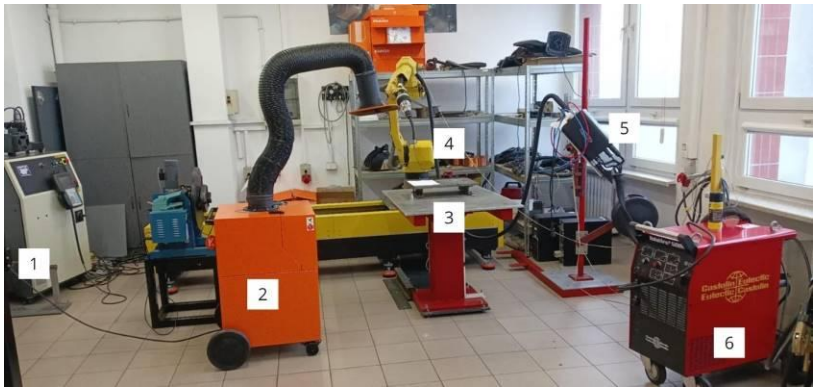

Fig. 11. A view of the robotic welding cell with FANUC Arc Mate 100iC welding robot

To determine and record the temperature, a PeakTech 5110 digital thermometer with a K-type thermocouple and a measuring range of -50°C to 1300°C was used for spot measurement. This thermometer enables rapid, direct measurement of surface temperature, Fig. 12. Measurements with the thermometer were used to calibrate the thermal imaging camera (determining the emissivity of the tested surfaces) and to determine the start time of deposition of the next layer, after achieving the required temperature.
The BOSCH GTC 600C thermal imaging camera was also used in the study, enabling imaging of temperature distribution across the tested surface and rapid, non-contact, point-by-point temperature measurement in real time (Fig. 12). The use of the thermal imaging camera enabled the capture of thermograms required for thermal analysis.
In the first stage of the study, single-bead deposition tests were performed with different parameters to determine the range of arc deposition parameters and the minimum current parameters, as well as minimum heat input ensuring stable wire deposition. Each subsequent bead was deposited after the substrate reached a temperature of 50°C at the location of the next bead. The parameters of the preliminary tests of deposition of single stringer beads are summarized in Table 1.
Based on previous tests and experience, a constant distance of 15 mm was established between the torch nozzle tip and the surface of the substrate (start plate).

Fig. 12. A view of the experimental stand with BOSCH GTC 600C thermal imaging camera (left) and PeakTech 5110 digital thermometer with a K-type thermocouple (right)

Table 1. Parameters of arc deposition of single straight beads and cross-sectional dimensions of beads

Bead No.	Traveling speed [m/min]	Set of current [A]	Real value of current [A]	Mean voltage [V]	Energy input* [kJ/cm]	Dimension of beads [mm]		
						Length	Width	Hight
1	0.2	60	62	21.2	3.95	98.05	7.85	2.2
2	0.3	60	61	21.5	2.62	98.2	6.25	2.2
3	0.4	60	60	21.3	1.92	100.7	5.9	1.8
4	0.5	60	60	21.5	1.55	100.8	4.15	1.55
5	0.5	80	84	23.1	2.33	101.9	6.95	1.6
6	0.5	100	104	24.1	3.0	99.5	8.38	1.45

*- Calculated value, not taking into account the efficiency of heat transfer to the material

Based on the analysis of preliminary test results, it was found that arc deposition of the wire was stable across the entire set parameter range. At the same time, it was found that increasing the traveling speed led to a reduction in the bead width and simultaneously a reduction in bead height, which was consistent with expectations. In turn, in the tested range of parameters, the increase in current intensity caused an increase in the bead width, but at the same time, a decrease in its height. Based on the obtained results, the initial parameters of test wall deposition were assumed: current intensity of 100 A, and travel speed of 0.5 m/min.

5. RESULTS

5.1. Analysis of thermal conditions during the deposition of single test beads

The study of thermal conditions began with the analysis of single straight beads deposited on the steel substrate at different parameters. The analysis aimed to determine the effect of current intensity on the maximum bead temperature immediately after the completion of deposition and on the temperature distribution on the bead surface. The results of temperature measurements at characteristic points for chosen test beads are presented in Table 2.

Fig. 13 shows a thermal image of bead No. 1, captured with a thermal imaging camera directly after the wire arc deposition. To precisely determine the values of temperature and temperature distribution across the bead surface, additional measurement points and measurement lines were marked, Fig. 13.

Table 2. Temperature values at characteristic points of chosen beads, Fig. 13, Table 1

Bead No.	Energy input* [kJ/cm]	Temperature at individual points [°C]			
		HS	M1	M2	M3
1	3.95	60.6	56.2	53.3	37.3
3	1.92	73.6	64.1	72.1	46.1
5	2.33	137.2	72.6	118.2	54.3
6	3.0	150.8	107.5	148.5	53.3

Remarks: HS – maximum temperature, M1, M2, M3 – additionally chosen points

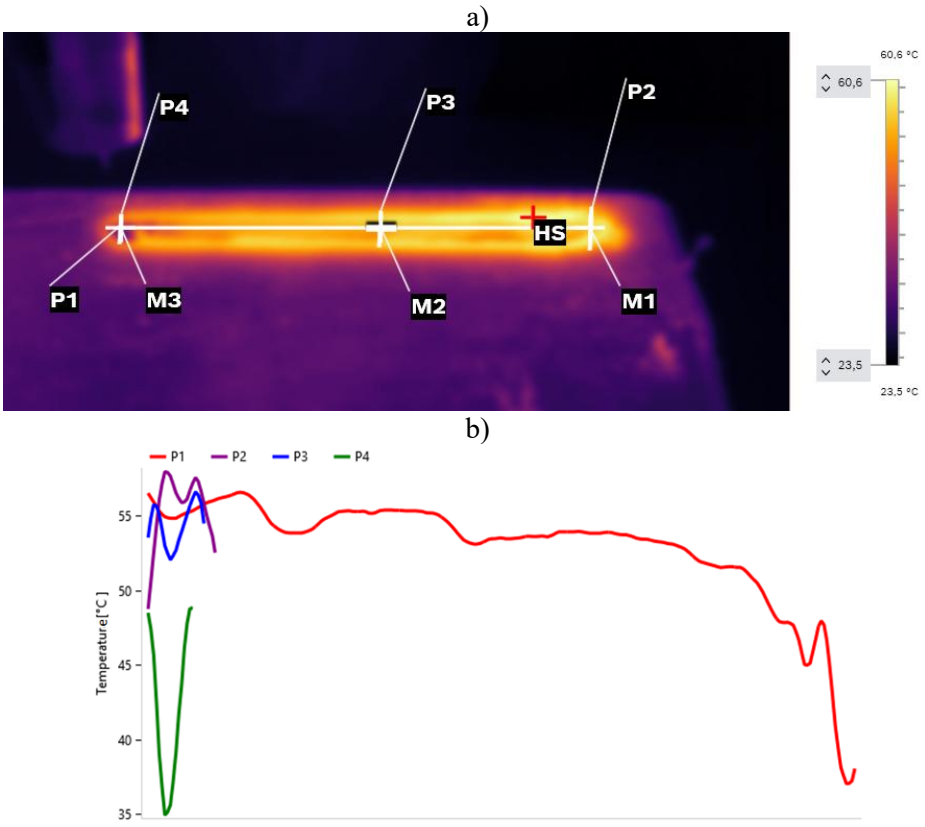

Fig. 13. Thermal image of bead No. 1 deposited at energy input 3.95 kJ/cm, and taken directly after deposition (a), and temperature distribution along measurement lines (b)

Bead No. 1 was deposited onto a steel starting plate, the initial temperature of which was approximately 22 degrees Celsius. The thermogram recorded directly after the bead was deposited (in practice, approximately 5 seconds after the end of the process) indicates that the highest temperature on the bead surface was 60.6°C. However, it was noticed that the temperature dropped rapidly. The single stringer bead, whose thermal image is shown in Fig. 13, was deposited from right to left. Therefore, the measurement line P1 plotted on the bead surface shows the highest temperature on the left side and a gradual temperature decrease toward the right. The additional lines P2-P4 indicate the temperature distribution across the bead, Fig. 13.

Fig. 14 shows the thermal image and temperature distributions of bead No. 3. As can be seen, although it was deposited at a much lower energy input of 1.92 kJ/cm, which is almost twice as low as that of bead No. 1, the surface temperature is higher.

This phenomenon may be related to the higher initial substrate temperature (approx. 50°C) before bead No. 3 was deposited, compared to bead No. 1, for which the deposition process began at ambient temperature (22°C), when the starting steel plate was not yet heated.

As can be seen in Table 2, although bead No. 5 and No. 6 were deposited at lower energy input than bead No. 1, and the initial temperature of the steel starting plate at the location of the next bead was kept the same, 50°C each time, the temperature of each subsequent bead after the deposition was completed was higher. Additionally, Fig. 15 shows a graph with the change of maximum temperature recorded directly after deposition

of each bead. This phenomenon can be explained by the accumulation of heat in the steel starting plate after deposition of each subsequent bead, and thus by a change in the conditions of heat conduction.
Based on thermal images recorded during the cooling of individual beads, the thermal cooling cycle was determined on the top surface of the bead, in the middle of its length. The results are shown in Fig. 16.

a)

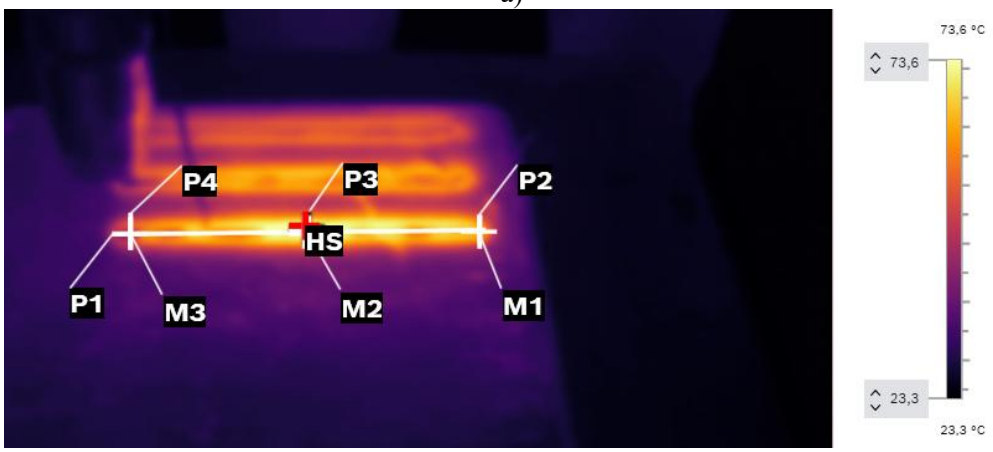

b)

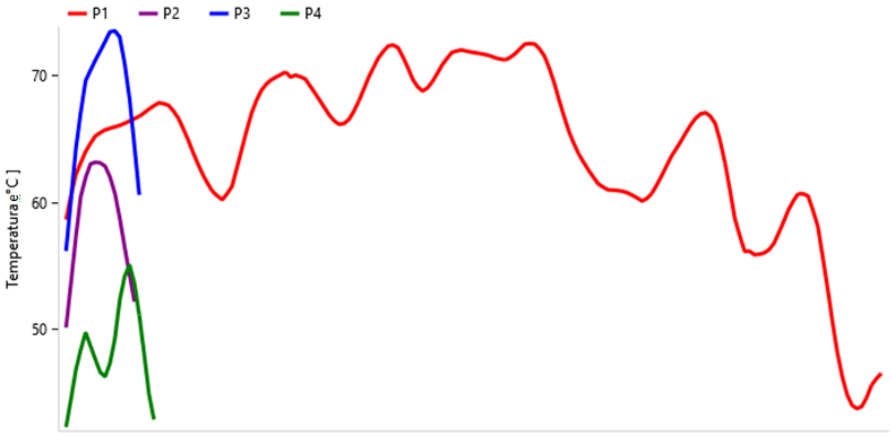

Fig. 14. Thermal image of bead No. 3 deposited at energy input 1.92 kJ/cm, and taken directly after deposition (a), and temperature distribution along measurement lines (b)

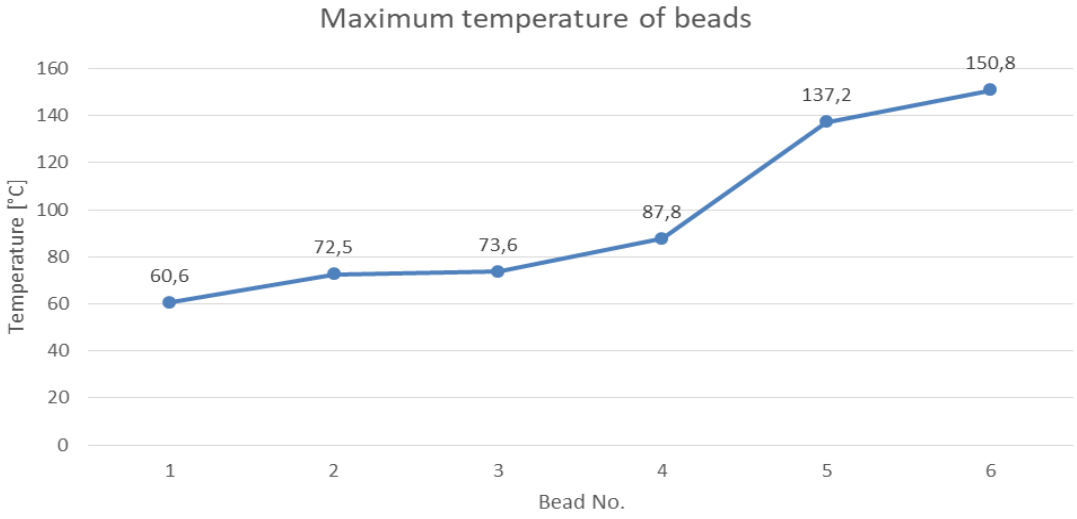

Fig. 15. A graph showing the change of maximum temperature recorded directly after deposition of each bead, Table 2

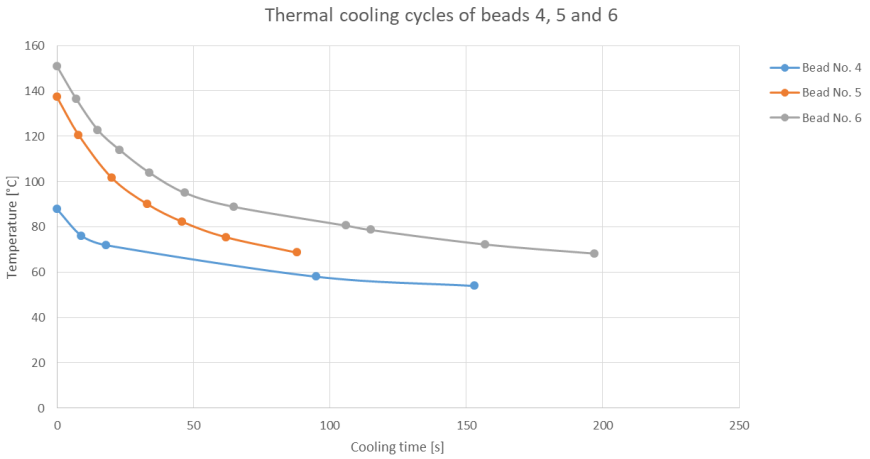

Fig. 16. Thermal cooling cycles of the deposited beads, Table 1

5.2. Analysis of thermal conditions during the deposition of the test wall

After preliminary tests and thermal analysis of straight beads, tests were carried out on the deposition of the vertical test wall. In the case of producing the vertical wall by deposition of individual beads, the increase in wall height was measured after each bead was deposited. The deposition parameters for two test walls are listed in Table 3 and Table 4, while the view of the test wall No. 1 is shown in Fig. 17, and macrostructure on cross-sections of the test wall in Fig. 20. The thermal conditions analysis methodology developed and tested for single stringer beads was used to analyse the thermal conditions during the deposition of beads/layers of the vertical test walls.

Fig. 18 shows the thermal images for the chosen beads taken during deposition of the multi-layer wall No. 1.

In turn, the thermal cooling cycles of individual beads/layers of the test wall no. 1 are shown in Fig. 18.

It should be noted that each subsequent bead was deposited after the substrate (partially completed wall) had reached a temperature of 50°C. The first thermal image for every individual bead was always taken directly after the deposited bead was completed.

It is evident from the thermal images, and especially from the cooling thermal cycles, that each subsequent bead had a higher temperature after the deposition was completed, and the cooling to the required temperature (50°C) of the substrate was longer. As can be seen in Fig. 19, the temperature determined for the individual beads/layers directly after the wire deposition process varies significantly, from 171-199°C for beads No. 1-3 up to 430°C for the bead No. 7. Therefore, continuous deposition of the test multi-layer wall, without cooling breaks, at unchanged parameters of the GMA arc deposition process, in the analysed range of parameters and technological conditions, is not possible, as it would lead to strong overheating of the produced wall. As can be seen in Table 3, beads No. 1 to 2 were deposited at the same energy input, at the current intensity of 100A, while from bead No. 7 onwards, the energy input was reduced by reducing the deposition current to 80A. Although the energy input was reduced by 20%, the wall temperature after deposition was still higher than for the previous beads deposited with a higher energy input and higher amperage, Fig. 19.

Table 3. Parameters of deposition of the individual eads/layers of multi-layer wall No. 1, Fig. 17, 20

Bead No.	Traveling speed [m/min]	Set of current [A]	Real value of current [A]	Mean voltage [V]	Vertical axis shift [mm]	Cooling time before deposition of the next bead [min]	Wall height [mm]
1	0.5	100	107	24.1	0	3	2
2	0.5	100	104	24.3	1.5	3	3
3	0.5	100	103	24	0.75	5	4.3
4	0.5	100	101	24	0.75	6	6.1
5	0.5	100	101	23.6	0.75	6	7.1
6	0.5	100	102	23.6	0.75	8	8.2
7	0.5	80	83	23	1	3	uneven height
8	0.5	80	81	23	1	1.5	uneven height
9	0.5	80	82	22.9	1	1.5	uneven height

Table 4. Parameters of deposition of the individual beads/layers of multi-layer wall No. 2, Fig. 20

Bead No.	Traveling speed [m/min]	Set of current [A]	Real value of current [A]	Mean voltage [V]	Vertical axis shift [mm]	Cooling time before deposition of the next bead [min]	Wall height [mm]
1	0.5	100	91	25	0	3	1,5
2	0.5	80	88	23	1	3	3,2
3	0.5	80	81	23.2	0.75	5	4.8
4	0.5	80	89	32.2	0.75	5	5.7
5	0.5	80	87	23.1	0.75	5	6.6
6	0.5	80	86	23.1	0.75	5	8.2
7	0.5	80	87	23.1	0.75	5	8.9
8	0.5	80	86	22.8	1	3	10.5
9	0.5	80	87	22.8	1	4	11.4

Fig. 17. A view of a vertical multi-layer wall (12.5 mm high) made by single-bead deposition, Table 3

a)

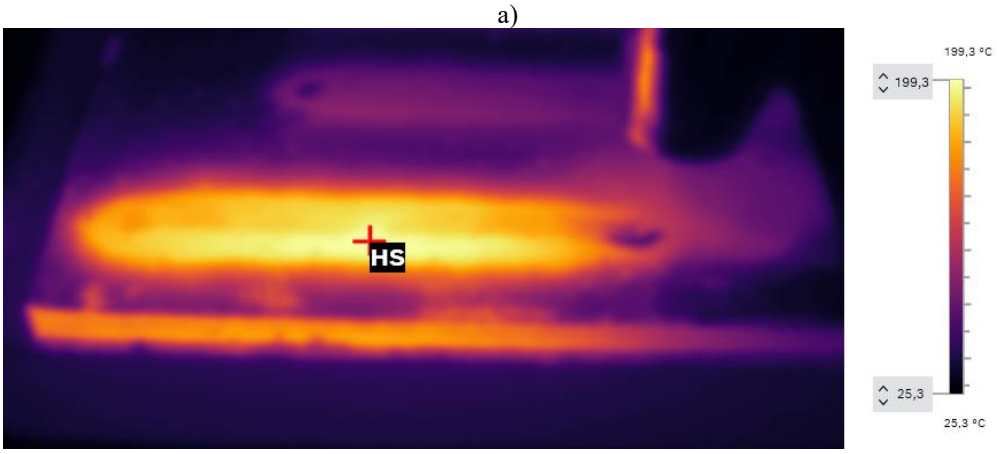

b)

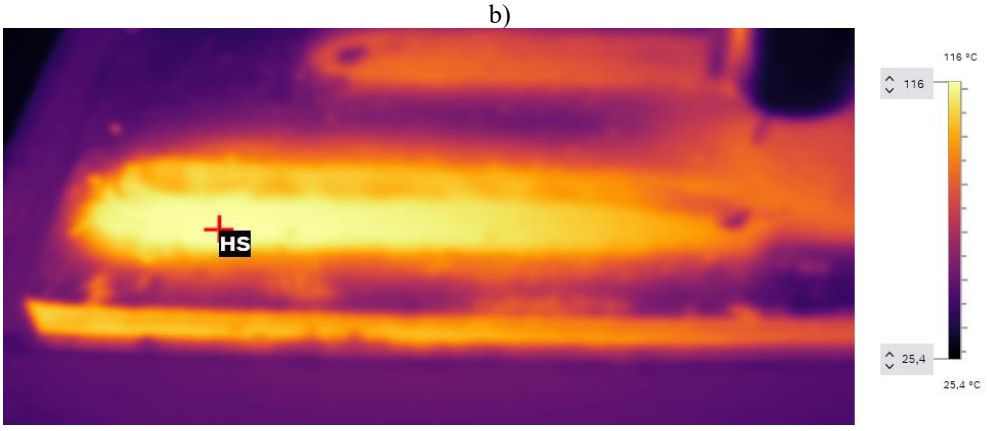

c)

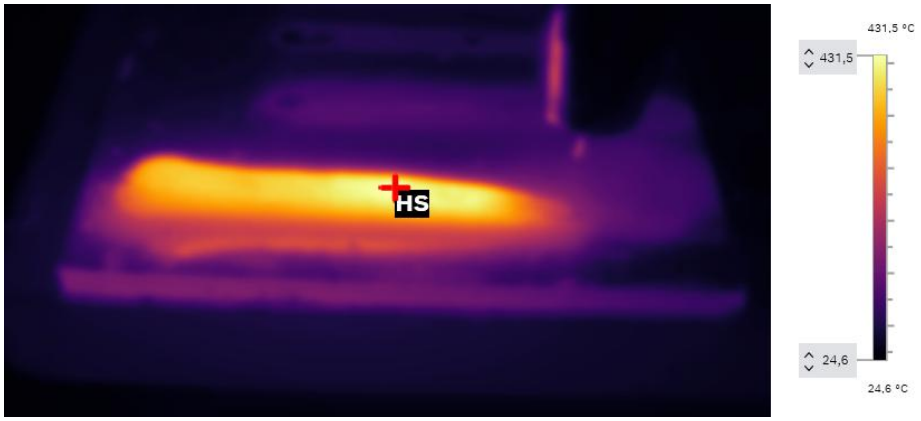

Fig. 18. Thermal images of subsequent beads/layers during deposition of multi-layer wall; a) bead No. 1, b) bead No. 4, and c) bead No. 7

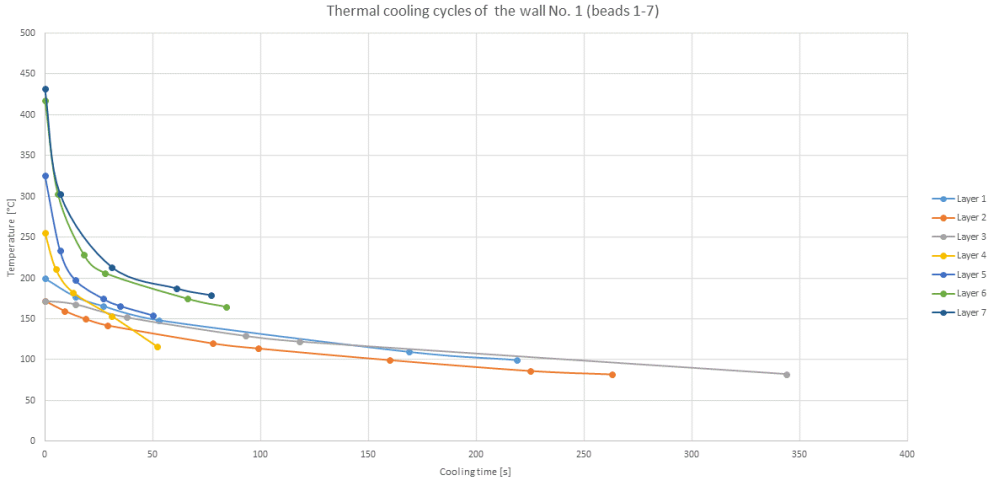

Fig. 19. Thermal cooling cycles of the deposited individual beads/layers of the multi-layer wall

5.2.1. Analysis of the shape and structure of test walls

Thanks to changing the energy input of deposition, the subsequent beads and by using different vertical shifts of the torch, depending on the actual height of individual beads/layers, the cross-section of the test walls is correct and has the same width along the entire height, Fig. 20.

The reason for this phenomenon is the change in the shape (geometry) of subsequent beads resulting from variable thermal conditions, as well as other conditions of subsequent bead formation on the surface of previous beads. It should be noted that the top surface of the bead (bead face) is not flat, but convex, which in turn requires melting the convex bead across its entire width and creating a melt pool that will support the volume of the molten metal and ensure height increase. This depends primarily on the surface tension forces of the melt pool; therefore, if the temperature is too high or the pool volume is too large, it will tend to drip down the side surfaces of the wall due to gravity.

Fig. 20, with the macrostructures in the cross-section of walls no. 1 and no. 2, also clearly shows the difference in the shape of the fusion lines of the individual beads. In the case of wall no. 1, the fusion line is clearly flat or slightly elliptical with a downward bend (slight depression), Fig. 20a. In turn, the fusion lines of the beads of wall no. 2 are clearly arc-shaped with an upward bend. In the case of test wall deposition, a lower energy input was used, starting from bead No. 2 (current intensity 80A). This reduced the substrate heating intensity, but the accuracy of the shape reproduction was also lower. The deviation of the wall from the vertical is clearly visible starting from the bead No. 5, Fig. 20.

For comparison, in the case of the test wall No. 1, a higher energy input was used (current intensity 100A), which makes the formation of subsequent layers more stable and repeatable, and the test wall has a lower deviation from the vertical.

Beside the difference in dimensional accuracy and vertical deviations, both walls are characterized by proper material continuity and a structure typical of layers deposited one on top of the other. The last layer clearly shows directional crystallization of columnar grains, which grow perpendicular to the fusion line (substrate). In turn, each previous layer is subjected to a thermal cycle as the next layer is deposited. This causes a distinct grain refinement in the previous layer, typical of normalization, as can be seen in Fig. 20. In the process of arc

deposition of test walls, a non-alloy steel wire containing 0.10% C, 1.11% Mn, 0.72% Si was used. The macroscopic photos in Fig. 20 clearly show that the last layers have a typical course-grained ferritic-pearlitic structure. In turn, the lower layers have recrystallized as a result of the thermal deposition cycle and have a fine-grained structure.

a)

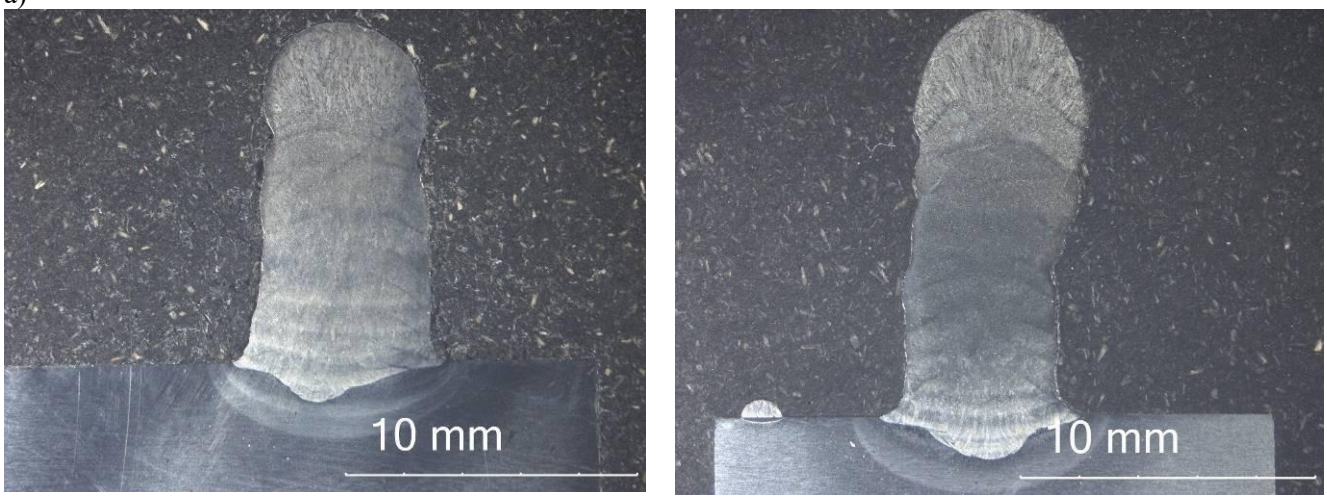

Fig. 20. Macrostructure of multi-layer walls: a) Wall No. 1, height 12.2 mm; b) Wall No. 2

6. CONCLUSIONS

Based on the analysis of thermal conditions during the additive manufacturing of test walls by arc deposition of unalloyed steel wire with a diameter of 1.0 mm, the following conclusions were drawn:

1. Arc deposition of successive wall beads changes the heat dissipation conditions, and as a result, the wall temperature increases after each bead is deposited. Ensuring the correct shape of the beads requires the use of cooling breaks and control of the wall temperature before starting the next bead deposition, as well as reducing the energy input for subsequent beads.
2. In the tested range of arc deposition parameters, energy input does not significantly affect the height of a single bead/layer, nor the width of the wall, but it does affect the width of the wall and the stability of the reproduction and repeatability of the shape and dimensions.
3. The proposed technique using a thermal imaging camera allows for the analysis of the entire area of the manufactured wall, as well as any 3D element, the determination of cooling cycles, and thus the forecasting/determination of the cooling break time. The developed thermographic research methodology shows potential in the analysis and adaptive control of the WAAM process.

Author Contributions: Conceptualization, AL, BB, SQ, YK; methodology and investigation, AL, YC; validation, MW, MZ; writing - original draft preparation, AL, S-N.M., FM-A, DC; writing - review and editing, DN, AL, CC; All authors have read and agreed to the published version of the manuscript.

Funding: This paper has received no external funding.

Conflicts of interest: There is no conflict of interest.

Acknowledgements: Publication supported by the Excellence Initiative - Research University programme implemented at the Silesian University of Technology, PBL 2025/26

6. REFERENCES

1. Vafadar A., Guzzomi F., Rassau A., Hayward K., (2021), *Advances in Metal Additive Manufacturing: A Review of Common Processes, Industrial Applications, and Current Challenges*, Appl. Sci., 11, 1213.
2. Li Y., et al., (2022), *Comprehensive review of wire arc additive manufacturing: Hardware system, physical process, monitoring, property characterization, application and future prospects*, Results Eng., 13, 100330.
3. Treutler K., Wesling V., (2021), *The Current State of Research of Wire Arc Additive Manufacturing (WAAM): A Review*, Appl. Sci., 11(18), 8619.
4. Mohebbi M. S., Kühl M., Ploshikhin V., (2020), *A thermo-capillary-gravity model for geometrical analysis of single-bead wire and arc additive manufacturing (WAAM)*, Int. J. Adv. Manuf. Technol., 109, 877–891.
5. Cunningham C. R., Flynn J. M., Shokrani A., Dhokia V., Newman S. T., (2018), *Strategies and processes for high quality wire arc additive manufacturing*, Addit. Manuf., 22, 672–686.

6. Gardner L., Kyvelou P., Herbert G., Buchanan C., (2020), *Testing and initial verification of the world's first metal 3D printed bridge*, J. Constr. Steel Res., 172, 106233.
7. Greer C., Nycz A., Noakes M., Richardson B., Post B., Kurfess T., Love L., (2019), *Introduction to the design rules for Metal Big Area Additive Manufacturing*, Addit. Manuf., 27, 159–166.
8. Kulikov A. A., Sidorova A. V., Balanovskiy A. E., (2020), *Process Design for the Wire Arc Additive Manufacturing of a Compressor Impeller*, IOP Conf. Ser. Mater. Sci. Eng., 969, 012098.
9. Bergmann J. P., Lange J., Hildebrand J., et al., (2020), *Herstellung von 3D-gedruckten Stahlknoten*, Stahlbau, 89, 956–969.
10. Panchenko O. V., Zhabrev L. A., Kurushkin D. V., Popovich A. A., (2019), *Macrostructure and Mechanical Properties of Al–Si, Al–Mg–Si, and Al–Mg–Mn Aluminum Alloys Produced by Electric Arc Additive Growth*, Met. Sci. Heat Treat., 60, 749–754.
11. Roy S., Shassere B., Yoder J., et al., (2020), *Mitigating Scatter in Mechanical Properties in AISI 410 Fabricated via Arc-Based Additive Manufacturing Process*, Materials, 13, 4855.
12. F. Lambiase, P. B. Yanala, F. Pace, A. Paoletti, (2025), *A state of the art review of wire arc additive manufacturing (WAAM)–part 1: process fundamentals, parameters and materials*, *The International Journal of Advanced Manufacturing Technology*, vol. 138, pp. 4965–4993, doi: 10.1007/s00170-025-15781-8.
13. Hassan A., et al., (2023), *A Comprehensive Review of Friction Stir Additive Manufacturing*, Materials, 16(7), 2723.
14. Chen Z., et al., (2025), *A comprehensive review and future perspectives of simulation approaches in wire arc additive manufacturing (WAAM)*, International Journal of Extreme Manufacturing, 7(2).
15. Liao S., et al., (2022), *Hybrid thermal modeling of additive manufacturing processes using physics-informed neural networks*, https://doi.org/10.48550/arXiv.2206.07756.
16. Pereira Álvarez P., et al., (2021), *Real-Time Data Assimilation in Welding Operations Using Local Probabilistic Surrogate Models and Thermal Imaging*, Mathematics, 9(18), 2263.
17. Mu H., He F., Yuan L., et al., (2024), *Online distortion simulation using generative machine learning models: A step toward digital twin of metallic additive manufacturing*, J. Ind. Inf. Integr., 38, 100563.
18. Miras H., et al., (2018), *Monte Carlo verification of radiotherapy treatments with CloudMC*, Radiat. Oncol., 13, 99.

Received: October 14th, 2025 / Received in the revised form: December 04 th, 2025 / Accepted: December 15th, 2025 / Paper available online: December 20th, 2025